UC Davis

Title

A pH-Driven Small-Molecule Nanotransformer Hijacks Lysosomes and Overcomes Autophagy-Induced Resistance in Cancer

Permalink

Journal

ISSN

Authors

Ma, Zhao
Lin, Kai
Tang, Menghuan
et al.

Publication Date

DOI

A pH-Driven Small-Molecule Nanotransformer Hijacks Lysosomes and Overcomes Autophagy-Induced Resistance in Cancer

Dr. Zhao Ma[a,b], **Dr. Kai Lin**[b,c], **Menghuan Tang**[b], **Mythili Ramachandran**[b], **Reng Qiu**[b], **Jin Li**[b], **Dr. Lucas N. Solano**[b], **Dr. Yanyu Huang**[b], **Dr. Cristabelle De Souza**[b], **Sara Abou-Adas**[b], **Dr. Bai Xiang**[b], **Prof. Lanwei Zhang**[c], **Prof. Minyong Li**[a], **Prof. Yuanpei Li**[b]

[a] Department of Medicinal Chemistry, Key Laboratory of Chemical Biology (MOE), School of Pharmaceutical Sciences, Cheeloo College of Medicine Shandong University, Jinan, Shandong 250012, China.

[b] Department of Biochemistry and Molecular Medicine, UC Davis Comprehensive Cancer Center, University of California Davis, Sacramento, CA 95817, USA

[c] College of Food Science and Engineering, Ocean University of China, Qingdao, Shandong 266003, China

Abstract

Smart conversion of supramolecular structures *in vivo* is an attractive strategy in cancer nanomedicine, which is usually achieved via specific peptide sequences. Here we developed a lysosomal targeting small-molecule conjugate, PBC, which self-assembles into nanoparticles at physiological pH and smartly converts to nanofibrils in lysosomes of tumor cells. Such transformation mechanically leads to lysosomal dysfunction, autophagy inhibition, and unusual cytoplasmic vacuolation, thus granting PBC a unique anticancer activity as a monotherapy. Importantly, the photo-activated PBC elicits significant phototoxicity to lysosomes and shows enormous advantages in overcoming autophagy-caused treatment resistance frequently occurring in conventional phototherapy. This improved phototherapy achieves a complete cure of oral cancer xenografts upon limited administration. Our work provides a new paradigm for the construction of nonpeptide nanotransformers with biomedical activities.

Graphical Abstract

The lysosomal targeting nonpeptide PBC (pheophorbide a–bisaminoquinoline conjugate) self-assembles into nanoparticles at physiological pH and then transforms into nanofibrils upon the trigger of lysosomal pH. Due to such shape transformation, PBC not only inhibits tumor growth as a single agent but also mediates a convenient photodynamic therapy with promise to overcome the autophagy-induced resistance and achieve tumor ablation.

mazhao@sdu.ed.cn, lypli@ucdavis.edu.

Conflict of Interest

Y.L. and Z.M. are the co-inventors on a pending patent application on the bisaminoquinoline-derived compound and the resulting nano-formulations. The remaining authors declare no competing interests.

Supporting information for this article is given via a link at the end of the document.
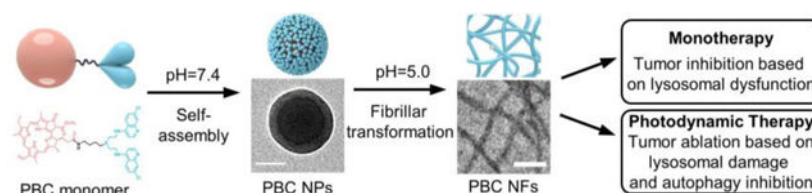
Introduction

Smart self-assembly of molecules into diverse nanostructures holds potential to enhance drug delivery and facilitate anticancer therapy.[1] In addition to the numerous *ex vivo* "pre-assembly/controlled-release" nanomedicines that have been extensively investigated in recent decades, *in situ* conversion of one supramolecular structure into another by endogenous stimuli is of growing interest in biomaterial fields.[2] These transformable nanomaterials preserve the advantages of preassembled nanoparticles in drug delivery and achieve desirable disposition characteristics within tumors.[3] A representative for *in situ* nanotransformation is from nanoparticles (NPs) to nanofibrils (NFs), which is usually constructed by using specific peptide segments or their derived conjugates according to the "*in vivo* self-assembly" strategy.[4] However, there are only a few peptide sequences available to support such shape transformation, and the peptide-intrinsic issues of stability and manufacturing might restrict their applications.[5] Discovery of nonpeptide molecules, especially small molecules, to construct controllable re-assemblies *in vivo* is a promising alternative to overcome the limitations of peptide-based nanotransformers.

Lysosomes are membrane-enclosed cytoplasmic organelles with an acidic interior comprising of over 60 different types of hydrolytic enzymes to break down cargos into their constituent molecules.[6] Advances in studies of lysosome function in malignant transformation and cancer progression have led to numerous therapeutic interventions targeting lysosomes that either directly kill cancer cells or sensitize them to other treatments. [7] Autophagy, an important lysosome-dependent pathway, is always harnessed by cancer cells to recycle their damaged macromolecules or organelles caused by the treatment, such as photodynamic therapy (PDT), which eventually result in cancer cell survival and treatment resistance.[8] Disrupting autophagy using lysosome inhibitors has become promising to address the autophagy-induced treatment resistance.[9]

Here we report a lysosome targeting Pheophorbide a (PA)-Bisaminoquinoline (BAQ) Conjugate, PBC, in which the hydrophobic PA moiety is used for aggregation inducing, fluorescence tracing, and photosensitization, while the cationic BAQ headgroup targets lysosome and initiates *in situ* protonation reaction (Figure 1a).[10] The ionizable PBC monomers self-assemble into PBC NPs under neutral aqueous conditions, which prolongs the systemic circulation and enhances the effective therapeutic concentrations in the tumor. Spectacularly, PBC NPs preferentially enter lysosomes in the tumor region, where they get

protonated and intelligently transform into NFs (Figure 1b).[11] The transformation impairs lysosomal functions, leading to autophagy blockade and cytoplasmic vacuolization, thus eliciting efficacious anticancer activity against oral tumors both *in vitro* and *in vivo* as a monotherapy (Figure 1c). Moreover, when activated by the appropriate photoirradiation, PBC NPs produce specific phototoxicity in lysosomes to boost the anti-proliferative effectiveness and overcome the autophagy-caused resistance (Figure 1c). The formed NFs allow the long-term sequestration of the photosensitizer at tumor sites, supporting multiple laser exposures upon a one-time drug administration. Due to these improvements, PBC NPs enable convenient and robust phototherapy, achieving a 100% complete cure rate against orthotopic oral cancer models under the more clinically translatable administration (2 doses totally). This small-molecule nanotransformable system offers not only a practical strategy to make the best of those inactive or slightly active compounds for anticancer therapy but also a promising approach to enhance the potency of photodynamic therapy (PDT).

Results and Discussion

To synthesize PBC monomer, BAQ was functionalized with the 4-amino butyl group, followed by the condensation reaction with PA (Figure S1, Supporting Information). The target compound and its primary intermediates were confirmed by NMR and MS spectra (Figure S2-S10, Supporting Information). PBC NPs were then prepared by nanoprecipitation under neutral aqueous solutions. Studies of transmission electron microscopy (TEM) and dynamic light scattering (DLS) revealed that PBC NPs have an average diameter of 127 nm and a positive surface charge of +38 mV (Figure S11a,b, Supporting Information). These 100% PBC NPs exhibited excellent stability in water, but not in PBS (Figure S11c, Supporting Information).[12] Subsequently, a small portion (20%) of DSPE-PEG2000 was added, which competently decreased the surface charge and improved the colloidal stability under various conditions without altering the size and critical aggregation concentration (Figure S11c–h, Supporting Information).[13] Since PBC serves as both the carrier and cargo, the self-assembling PBC NPs gained a high drug-loading capacity (over 80%, wt). Considering the improved stability under physiological conditions, we used the PEGylated PBC NPs in the following studies.

PBC NPs are designed to target the lysosome, where the BAQ headgroup of the PBC monomer would get protonated completely. To determine changes in the self-assembling states of PBC upon protonation (Figure 2a), we performed the ultrafiltration studies using 10 kDa molecular weight cut-off filtration membrane. At pH 7.4, PBC NPs were retained in the supernatant and displayed the Tyndall effect and uniform spherical nanostructures (Figure 2b).[14] By contrast, though the Tyndall effect disappeared after protonation at pH 5.0, PBC remained trapped in the supernatant (Figure 2b). This phenomenon indicates that the protonation converts PBC from NPs into other aggregates, which were subsequently identified as PBC NFs with a diameter of ~10 nm (Figure 2b). Since PEGylated and non-PEGylated PBC NPs generated similar NFs, we confirmed that DSPE-PEG2000 neither affects this process nor is present in the formed PBC NFs (Figure S12, Supporting Information). As a simple small-molecule compound conjugate, it is fascinating that PBC could achieve such conversion between supramolecular structures.

To further trace the transition process, we prepared a series of PBS solutions with a pH gradient from 7.4 to 4.0 to treat PBC NPs and subjected them to DLS analysis and TEM examination. PBC NPs exhibited unimodal signals and spherical nanostructures under near-neutral conditions (pH 7.4–6.0), whereas they displayed multimodal signals and nanofibrillar structures under more acidic conditions (pH 5.5–4.0) (Figure 2c). The critical pH for the transition is 5.5, at which an intermediate state with compatible NPs and NFs was detectable (Figure 2d, and Figure S13a, Supporting Information). In the time-course measurements, multimodal DLS signals and nanofibrillar structures were detected in 1 h after acidification, indicating that the conversion from PBC NPs to PBC NFs occurs quickly (Figure 2e,f, and Figure S13b, Supporting Information). If self-assembled at pH 5.0, PBC monomers could form NFs directly, and the formed NFs could not convert to NPs reversely when the pH was adjusted back to 7.4 (Figure S14, Supporting Information).

The characteristic UV/Vis absorption and fluorescence peaks of PA group underwent a redshift when PBC monomers aggregated into NPs or NFs (Figure 2g,h), which might be attributed to the π-π interactions of PA structures under aggregation states.[15] Furthermore, the bathochromic scale of PBC NFs was larger than that of PBC NPs, suggesting that an ordered J-aggregation of PBC occurred during the transition.[16] This was also confirmed by circular dichroism (CD) spectroscopy, in which PBC NFs showed the peak corresponding to the UV-Vis absorption while it was void for the monomeric and nanoparticulated PBC (Figure 2i).[16] As a control, BAQ16 NPs not containing PA moiety were dissociated into small molecules after acidification (Figure S15, Supporting Information), suggesting that the bulk PA group capable of strong hydrophobicity interaction and π-π stacking is essential for the assembly and transformation of PBC aggregates. According to the hypothesis by Israelachvili et al.,[17] the spherical or fibrillar organization of PBC can be interpreted as the packing of molecules of effective conical shape or wedge shape, respectively. At pH 7.4, the surface area of hydrophilic BAQ headgroup is relatively larger due to hydration so that PBC occupies an effective volume of a cone and tends to form NPs. By contrast, at pH 5.0, binding of a counterion over multiple protonated PBC molecules leads to an effective shape similar to that of a wedge, which breaks the local symmetry of the original assembly and promotes the change in shape into NFs.[18]

Our previous findings have demonstrated that the BAQ derivatives that function in the lysosome have a typical structure-activity relationship (SAR), in which the cytotoxicity gradually decreases as their R substituent is over-extend (Figure 3a).[14] PBC NPs, Lys05, and three control BAQ NPs (BAQ15, BAQ16, and BAQ18) were subjected to cytotoxicity assessments using OSC-3 oral squamous cell carcinoma cells. The three BAQ NPs highly conformed to the SAR above, while PBC having the largest R substituent among all groups did not, because it is dramatically equivalent to Lys05 and much better than three BAQ NPs (Figure 3b).[14] Such unusual SAR also generalizes to other cancerous cell types, underlining the unique fate of PBC in cancerous cells (Figure S16, Supporting Information). Compared to cancerous cells, the noncancerous cells showed relatively low sensitivity to PBC NPs (Figure S16, Supporting Information). This selectivity could be attributed to that cancer cells contain more lysosomes and could take up more PBC NPs than normal cells. (Figure S17, Supporting Information).[19] Considering the aggregation state difference in lysosomes of PBC and other BAQ derivatives, we speculated that the unconventional

cytotoxicity of PBC NPs may be ascribed to their unique re-assembly behavior in the lysosome.[20]

To validate the hypothesis, the cellular entry pathway of PBC NPs was interrogated firstly. Among four endocytosis inhibitors, only genistein significantly decreased the uptake of PBC NPs into OSC-3 cells, implicating that the caveolae-mediated endocytosis pathway was involved (Figure S18, Supporting Information).[18b] After endocytosis, PBC NPs were accumulated in lysosomes of OSC-3 cells and caused lysosomal deacidification through *in situ* protonation (Figure S19 and S20, Supporting Information).[21] Subsequently, the shape transformation in lysosomes of PBC NPs was observed under TEM. OSC-3 cells treated with PBC NPs showed apparent nanofibrillar structures in the lysosome, whereas none of such structures were observed in other groups (Figure 3c). This is a crucial piece of evidence that substantiates the intra-lysosomal conversation from PBC NPs to PBC NFs. In addition, changes in lysosomal morphology may signify lysosomal defects.[22] The lysosomes containing PBC NFs displayed inhomogeneous matrix distribution, implying the lysosomal dysfunction caused by PBC NFs (Figure 3c).

In the measurements of lysosomal integrity, we found that treatment with PBC NPs caused the leakage of acridine orange from lysosomes to the cytosol, indicating the ability of PBC in inducing lysosomal membrane instability (Figure 3d). This is owing to that PBC NFs possessing a high surface-area-to-volume ratio and positive surface chargers could strongly bind to the negatively charged lysosomal membrane. Interestingly, a long (16 h) incubation of PBC NPs caused the visible vacuolization in OSC-3 cells (Figure 3e). These vacuoles completely excluded signals of endoplasmic reticulum (ER) and mitochondria but were closely associated with lysosomes (Figure S21, Supporting Information). The diffuse staining patterns of fluorescent dextran (a macropinocytosis probe) restricted in the vacuole area further indicated that these vacuoles were derived from macropinosome and endosome compartments (Figure 3f).[23] Under a normal condition, these compartments should fuse with lysosomes, but when PBC NFs that could induce lysosome dysfunction are present, the fusion would be inhibited, therefore, the vacuoles are formed[24]. We also evaluated the effects of PBC NPs on autophagy pathway by detecting the levels of the autophagosome marker (the lipid-modified form of microtubule-associated protein 1 light chain 3B, LC3B-II) and the autophagy substrate (SQSTM1/p62). If inducing autophagy, LC3-II and p62 would be increased and decreased, respectively, while both LC3-II and p62 should be increased when inhibiting autophagy. PBC NPs demonstrated a considerable effect on inhibiting autophagy as the OSC-3 cells treated by them showed increased levels of LC3B-II and p62 (Figure 3g). Unlike Lys05 which induced appreciable levels of apoptosis and necrosis, PBC-caused cancer cell death bypassed the classical apoptosis and necrosis pathways, opening up a new approach against the classical apoptosis- and necrosis-resistant cancers (Figure 3h).[24]

The *in vivo* pharmacokinetic study using iv injection into Sprague–Dawley rats revealed that PBC NPs have a more prolonged blood circulation time than the small-molecule PA with 26 times higher area under the curve (AUC) (Figure 4a, and Figure S22, Table S1, Supporting Information). The orthotopic oral OSC-3 tumor-bearing nude mice were employed to ascertain the biodistribution of PBC NPs upon the single-dose iv administration. Both the

in vivo and ex vivo fluorescence imaging results indicated that PBC NPs could be retained in tumors for 6 d while PA was almost cleared from tumors within 24 h (Figure 4b,c). The quantitative fluorescence intensity of tissues that were collected at 72 h further confirmed the distinguishable biodistribution of PBC NPs in the tumor area compared to the normal tissues (Figure 4d). Confocal imaging of OSC-3 tumor cryosection further validated the existence in tumor tissue of PBC assemblies and their colocalization with lysosomes (Figure 4e). The multi-dose toxicity of PBC NPs was assessed in mice after a continuous treatment of a total of 7 doses by every two days. Both H&E staining patterns of normal organs and hematologic tests did not exhibit apparent abnormal alterations among various groups of mice, suggesting that the therapeutic dose of 20 mg kg^{-1} of PBC NPs was well tolerated by mice when administered by tail vein (Figure S23–25, Supporting Information).

To investigate the antitumor effects *in vivo* of PBC as a single agent, nude mice bearing orthotopic OSC-3 tumors were randomly assigned into five groups when the average tumor volume reached 50 mm^3, and were administered intravenously every two days with PBS, PA, Lys05, BAQ16 NPs or PBC NPs, respectively. As a result, PBC NPs significantly decelerated the growth of OSC-3 tumors and elicited a more efficacious therapeutic outcome than Lys05; By contrast, BAQ16 NPs and PA did not impede tumor growth at all (Figure 4f). During the treatments, none of the groups caused a decrease in bodyweight (Figure 4g).

To better understand the function of PBC NPs *in vivo*, the tumor tissues from each group were harvested after 7 injections of PBC NPs for the tissue-level analysis. By using immunoblotting, we found that both p62 and LC3B-II were increased after treatment with PBC NPs, implicating their effective autophagy inhibiting effect in tumors (Figure 4h). A series of histological assays were conducted to detect cancer cell states and the expression of certain proteins. As depicted in Figure 4i, the tumor treated with PBC NPs exhibited the more cell damage (H&E), inhibition of autophagy degradation (increased LC3B expression), high vacuolation (increased Rab7 expression), and lower proliferative activity (decreased Ki67 expression), indicating that PBC NPs were effective in arresting tumor growth *in vivo* through inhibiting autophagy and inducing vacuolation.

PDT is an alternative tumor-ablative treatment modality.[25] However, it has been reported that the conventional PDT would upregulate autophagy in cancer cells to cause treatment resistance.[9, 26] Using a tandem RFP-GFP-LC3B reporter, we assessed the autophagic flux in OSC-3 cells exposed to the photosensitization of PA. This conventional PDT caused an acute induction of autophagolysosomal (RFP$^+$ only) or autophagosomal (RFP$^+$GFP$^+$) puncta, suggesting an increased autophagy flux (Figure 5a). This change was accompanied by a rapid increase of LC3B-II and a robust reduction of p62 (Figure 5b).[27] Inhibiting autophagy using Lys05 could potentiate the anti-proliferative effect of PDT (Figure 5c,d, and Figure S26, Supporting Information). These data demonstrate that the conventional PDT could activate autophagy which, in turn, causes treatment resistance or failure.

Considering the lysosomal targeting of PBC, we envisioned that the PDT mediated by PBC NPs could overcome the corresponding treatment resistance via disrupting lysosomes. [28] The impact of pH on the photosensitization efficiency was investigated using singlet oxygen ($^1O_2$) sensor green (SOSG). When pH decreased, PA showed a drop in the singlet

oxygen production as its solubility falls (Figure S27, Supporting Information); By contrast, PBC NPs at pH 5.0 enabled more $^1O_2$ production than at pH 7.4 due to the increased surface-area-to-volume ratio following the shape transformation (Figure 5e). To measure the intracellular level of reactive oxygen species (ROS), OSC-3 cells preloaded with PBC NPs and 2',7'-dichlorofluorescein diacetate (DCF-DA) were subjected to flow cytometry analysis or confocal imaging at 30 min after laser irradiation. PBC plus laser caused a sharp increase of ROS production in cells, approximately 12 times that produced by PA and laser (Figure 5f, and Figure S28, Supporting Information). Imaging with AO or fluorescent dextran manifested that the lysosomal integrity of OSC-3 cells treated with PBC and laser (1 μM) was quickly damaged (Figure S29, Supporting Information). Immunoblotting demonstrated that PBC NPs plus laser caused a dose-dependent autophagy inhibition, which was equally as potent as that of 10-fold concentrations of the well-characterized autophagy inhibitor Lys05 and was opposed to the effect of laser-illuminated PA (Figure 5g). The TEM results (Figure 5h) indicated that the OSC-3 cells treated with PBC NPs and laser were strewn with autophagic vacuoles in the cytoplasm. Similar to the traditional photosensitizers, PBC NPs could also activate the upstream genes of autophagy when performing PDT (Figure S30, Supporting Information).[29] However, due to its specific phototoxicity in lysosomes, the degradation step is impeded, eventually leading to autophagy blockage. The PDT mediated by PBC NPs exhibited considerable advantages in cytotoxicity and apoptosis induction compared with other treatments (Figure 5i and Figure S31-34, Supporting Information). In particular, in presence of rapamycin, an autophagy inducer, the anticancer efficiency of PDT mediated by PBC NPs was not affected, which shows a great difference from that of PA and represents a promising modality to address the autophagy-induced treatment resistance that frequently occurs in the conventional PDT (Figure S35, Supporting Information).

The aforementioned findings have proved that the transformable PBC NPs enable an excellent accumulation and extended retention in tumors. We also confirmed that PBC NFs are well photostable even after a total of 8 cycles of laser exposures (Figure S36, Supporting Information).[30] These results indicate that PBC NPs are appropriate to be charged with multiple photodynamic reactions upon a one-time injection of our material to achieve a convenient and effective PDT *in vivo*. Intratumoral ROS production over time induced by photosensitization of single-dose PBC NPs was determined. OSC-3 tumors were harvested at the predetermined time points, stained with DCF-DA, and irradiated with laser, followed by fluorescent imaging. Treatment with PBC NPs elicited sustainable release of ROS upon laser exposure, showing a significant increase compared with treatment with PA (Figure 6a and Figure S37, Supporting Information). In addition, we also measured the temperature of the laser-treated tumors and found that PBC NPs did not cause a significant increase in tumoral temperature under the set laser condition (Figure S38, Supporting Information), indicating that the photothermal effect was negligible in our studies.

Based on the findings above, we proposed a PBC-based PDT schedule for the animal treatment study, including two cycles of drug and laser treatments. For each cycle, total 4 times of laser irradiations (at 24 h, 48 h, 72 h, and 96 h, respectively) were performed following the one-time injection of PBC NPs by tail vein (Figure 6b). Mice bearing the orthotopic OSC-3 xenograft with an average volume of 50 mm^3, were divided into 4 groups and treated as indicated. Tumors were completed cured after the predetermined

treatments using PBC NPs, whereas treatment with PA plus laser only obtained a slight inhibition of tumor growth (Figure 6c). Similar to the previous data, the influence of PBC NPs plus laser on mice bodyweight was negligible, further confirming the safety of the treatment (Figure 6d). Immunoblotting indicated that the conventional PDT using PA as the photosensitizer induced autophagy in the tumor, while our PBC NPs mediated phototherapy caused intratumoral autophagy blockade effectively, which was more potent than Lys05 (Figure 6e). These results were also supported by the IHC staining of tumor sections with LAMP-1 and LC3B. The decreased level of LAMP-1, which means less lysosome amount in the tumor, and the increased expression of LC3B, which means the autophagy degradation is inhibited in the tumor, were observable in the PBC NPs and laser-treated tumors (Figure 6f). Moreover, as indicated by H&E and Ki67 staining, tumors from the PBC NPs plus laser group showed decreased proliferative activities (Figure 6f). Given their advantages of extended retention and overcoming autophagy resistance in tumors, PBC could act as a promising photodynamic therapeutic tool for tumor cell killing *in vivo*.

Conclusion

Nanostructural assemblies can directly interact with cellular components and control cellular fate. Constructing nanostructures with biofunctions in tumor cells is an attractive approach in development of intelligent and versatile anticancer nanomedicine. In this study, we have developed a lysosomal targeting nonpeptide small-molecule conjugate, PBC, to construct specific nanotransformers of anticancer activity. The uniform NPs formed by PBC molecules under the neutral condition could smartly convert into NFs when getting protonated in the lysosomes of tumor cells, thus achieving a phase transformation from NPs to NFs. The supramolecular assembly and proton-driven re-assembly not only make the small molecule hijack the lysosome to exert unique activities against cancer cells, but also improve biodistribution and extend retention at the tumor sites. Thus, PBC nanotransformer can effectively suppress tumor growth as a monotherapy. Also, PBC-mediated PDT could overcome the inherent autophagy-caused treatment resistance in conventional PDT to eliminate tumors conveniently and efficaciously. We believe that this versatile nanotransformer will inspire the discovery of nonpeptide building blocks to design diverse nanotransformers and contribute to drug development.

Supplementary Material

Refer to Web version on PubMed Central for supplementary material.

Acknowledgements

References

[1]. a)Meel R. v. d., Sulheim E, Shi Y, Kiessling F, Mulder WJM, Lammers T, Nat. Nanotech 2019, 14, 1007–1017;b)Wang H, Feng Z, Xu B, Chem. Soc. Rev 2017, 46, 2421–2436. [PubMed: 28357433]

[2]. a)Lu Y, Aimetti AA, Langer R, Gu Z, Nat. Rev. Cancer 2016, 2, 16075;b)Webber MJ, Appel EA, Meijer EW, Langer R, Nat. Mater 2016, 15, 13–26. [PubMed: 26681596]

[3]. a)Mamuti M, Zheng R, An H-W, Wang H, Nano Today 2021, 36, 101036;b)Wang Y, Li S, Wang X, Chen Q, He Z, Luo C, Sun J, Biomaterials 2021, 271, 120737.

[4]. a)He P-P, Li X-D, Wang L, Wang H, Acc. Chem. Res 2019, 52, 367–378; [PubMed: 30653298] b)Xu C, Yu Y, Sun Y, Kong L, Yang C, Hu M, Yang T, Zhang J, Hu Q, Zhang Z, Adv. Funct. Mater 2019, 29, 1905213.

[5]. Fosgerau K, Hoffmann T, Drug Discov. Today 2015, 20, 122–128. [PubMed: 25450771]

[6]. Lawrence RE, Zoncu R, Nat. Cell Biol 2019, 21, 133–142. [PubMed: 30602725]

[7]. a)Ballabio A, Bonifacino JS, Nat. Rev. Mol. Cell Biol 2020, 21, 101–118; [PubMed: 31768005] b)Fehrenbacher N, Jäättelä M, Cancer Res. 2005, 65, 2993–2995; [PubMed: 15833821] cAppelqvist H, Wäster P, Kågedal K, Öllinger K, J. Mol. Cell Biol 2013, 5, 214–226. [PubMed: 23918283]

[8]. Levy JMM, Towers CG, Thorburn A, Nat. Rev. Cancer 2017, 17, 528–542. [PubMed: 28751651]

[9]. Wei M-F, Chen M-W, Chen K-C, Lou P-J, Lin SY-F, Hung S-C, Hsiao M, Yao C-J, Shieh M-J, Autophagy 2014, 10, 1179–1192. [PubMed: 24905352]

[10]. a)Rajora MA, Lou JWH, Zheng G, Chem. Soc. Rev 2017, 46, 6433–6469; [PubMed: 29048439] b)McAfee Q, Zhang Z, Samanta A, Levi SM, Ma X-H, Piao S, Lynch JP, Uehara T, Sepulveda AR, Davis LE, Winkler JD, Amaravadi RK, Proc. Natl Acad. Sci. USA 2012, 109, 8253–8258. [PubMed: 22566612]

[11]. a)Miao L, Li L, Huang Y, Delcassian D, Chahal J, Han J, Shi Y, Sadtler K, Gao W, Lin J, Doloff JC, Langer R, Anderson DG, Nat. Biotechnol 2019, 37, 1174–1185; [PubMed: 31570898] b)Ball RL, Hajj KA, Vizelman J, Bajaj P, Whitehead KA, Nano Lett. 2018, 6, 3814–3822.

[12]. Sun B, Luo C, Zhang X, Guo M, Sun M, Yu H, Chen Q, Yang W, Wang M, Zuo S, Chen P, Kan Q, Zhang H, Wang Y, He Z, Sun J, Nat. Commun 2019, 10, 3211. [PubMed: 31324811]

[13]. Yang Y, Sun B, Zuo S, Li X, Zhou S, Li L, Luo C, Liu H, Cheng M, Wang Y, Wang S, He Z, Sun J, Sci. Adv 2020, 6, eabc1725.

[14]. Ma Z, Li J, Lin K, Ramachandran M, Zhang D, Showalter M, De Souza C, Lindstrom A, Solano LN, Jia B, Urayama S, Duan Y, Fiehn O, Lin T.-y., Li M, Li Y, Nat. Commun 2020, 11, 4615. [PubMed: 32934241]

[15]. Zheng J, Fan R, Wu H, Yao H, Yan Y, Liu J, Ran L, Sun Z, Yi L, Dang L, Gan P, Zheng P, Yang T, Zhang Y, Tang T, Wang Y, Nat. Commun 2019, 10, 1604. [PubMed: 30962431]

[16]. Huynh E, Leung BYC, Helfield BL, Shakiba M, Gandier J-A, Jin CS, Master ER, Wilson BC, Goertz DE, Zheng G, Nat. Nanotechnol 2015, 10, 325–332. [PubMed: 25822929]

[17]. Lombardo D, Kiselev MA, Magazù S, Calandra P, Adv. Condens. Matter Phys 2015, 2015, 151683.

[18]. a)Schäfer K, Kolli HB, Killingmoe Christensen M, Bore SL, Diezemann G, Gauss J, Milano G, Lund R, Cascella M, Angew. Chem. Int. Ed 2020, 59, 18591–18598;b)Lin K, Ma Z, Li J, Tang M, Lindstrom A, Ramachandran M, Zhu S, Lin T.-y., Zhang L, Li Y, Adv. Funct. Mat 2021, 31, 2008460.

[19]. Dielschneider RF, Henson ES, Gibson SB, Oxid. Med. Cell Longev 2017, 2017, 3749157.

[20]. a)Pires RA, Abul-Haija YM, Costa DS, Novoa-Carballal R, Reis RL, Ulijn RV, Pashkuleva I, J. Am. Chem. Soc 2015, 137, 576–579; [PubMed: 25539667] b)Borkowska M, Siek M, Kolygina DV, Sobolev YI, Lach S, Kumar S, Cho Y-K, Kandere-Grzybowska K, Grzybowski BA, Nat. Nanotechnol 2020, 15, 331–341. [PubMed: 32203435]

[21]. Tang M, Lin K, Ramachandran M, Li L, Zou H, Zheng H, Ma Z, Li Y, Acta Pharm. Sin. B 2022, 12, 2672–2682. [PubMed: 35755275]

[22]. Lüllmann-Rauch R, in Lysosomes, Springer US, Boston, MA, 2005, pp. 1–16.

[23]. a)Commisso C, Flinn RJ, Bar-Sagi D, Nat. Protoc 2014, 9, 182–192; [PubMed: 24385148] b)Schink KO, Tan KW, Spangenberg H, Martorana D, Sneeggen M, Stévenin V, Enninga J, Campsteijn C, Raiborg C, Stenmark H, Nat. Commun 2021, 12, 6577. [PubMed: 34772942]

[24]. Huang W, Sun X, Li Y, He Z, Li L, Deng Z, Huang X, Han S, Zhang T, Zhong J, Wang Z, Xu Q, Zhang J, Deng X, J. Med. Chem 2018, 61, 5424–5434. [PubMed: 29878764]

[25]. Li X, Lovell JF, Yoon J, Chen X, Nat. Rev. Clin. Oncol 2020, 17, 657–674. [PubMed: 32699309]

[26]. Dewaele M, Martinet W, Rubio N, Verfaillie T, de Witte PA, Piette J, Agostinis P, J. Cell. Mol. Med 2011, 15, 1402–1414; [PubMed: 20626525] b Domagala A, Stachura J, Gabrysiak M, Muchowicz A, Zagozdzon R, Golab J, Firczuk M, BMC Cancer 2018, 18, 210. [PubMed: 29463237]

[27]. Ji Y, Liu X, Li J, Xie X, Huang M, Jiang J, Liao Y-P, Donahue T, Meng H, Nat. Commun 2020, 11, 4249. [PubMed: 32843618]

[28]. Kessel D, J. Natl. Compr. Cancer Network 2012, 10, S56–S59.

[29]. Martins WK, Belotto R, Silva MN, Grasso D, Suriani MD, Lavor TS, Itri R, Baptista MS, Tsubone TM, Front. Oncol 2021, 10, 610472.

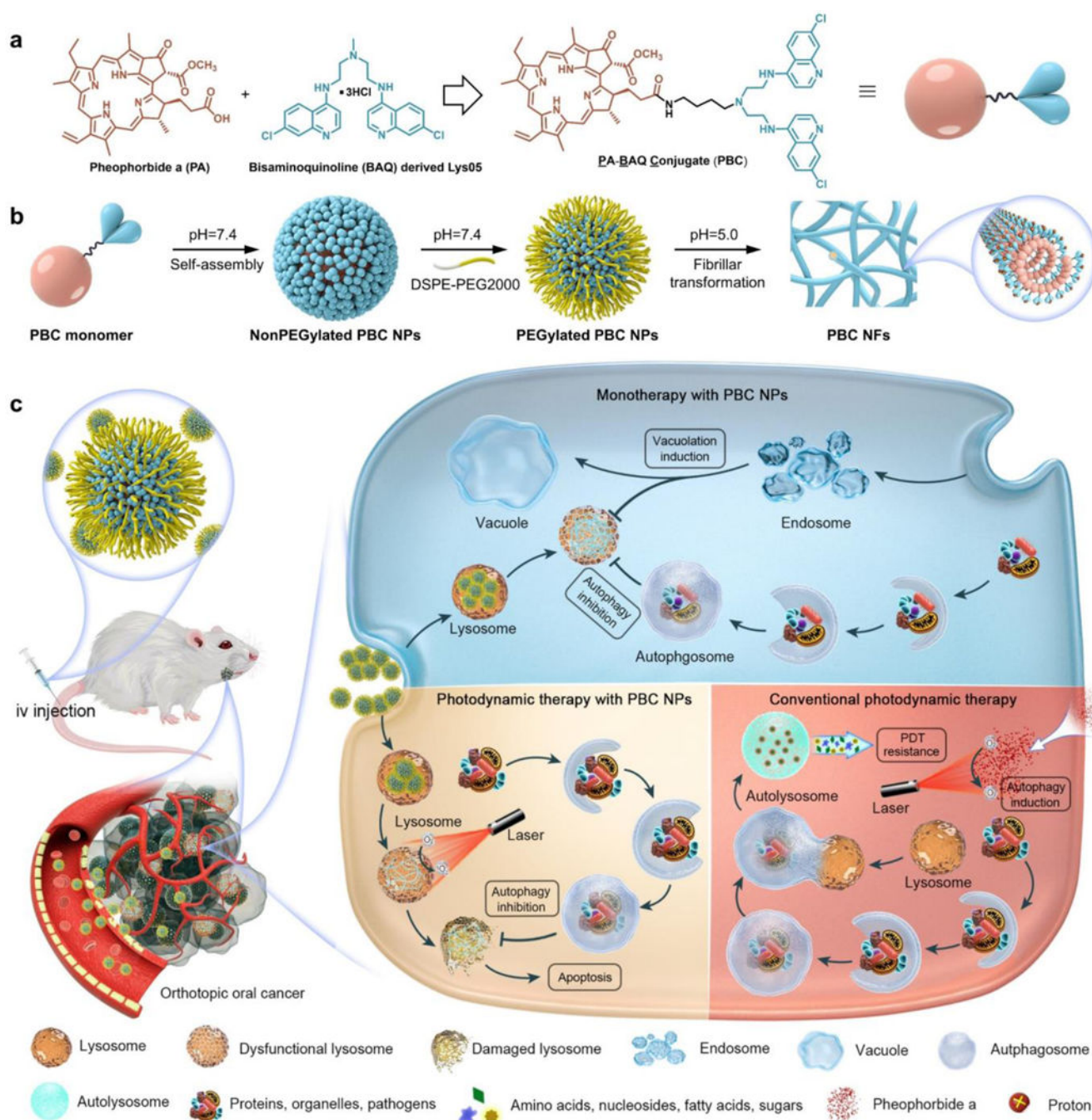[30]. Li W, Ma Z, Chen J, Dong G, Du L, Li M, Anal. Chem 2022, 94, 7021–7028. [PubMed: 35504022]

Figure 1.
Schematic illustration of the lysosomal pH-responsive small molecule-based nanotransformer. a) Chemical structure of PBC monomer. b) Self-assembling and transformation behaviors of PBC at pH 7.4 and pH 5.0. c) In the orthotopic oral cancer model, PBC NPs could not only cause cancer cell death as a monotherapy through the lysosomal dysfunction, autophagy inhibition, and cytoplasmic vacuolization induced by the morphologic transformation, but also mediate a powerful photodynamic therapy (PDT) with

promises to overcome the inherent autophagy-induced treatment resistance in conventional PDT and achieve tumor ablation.
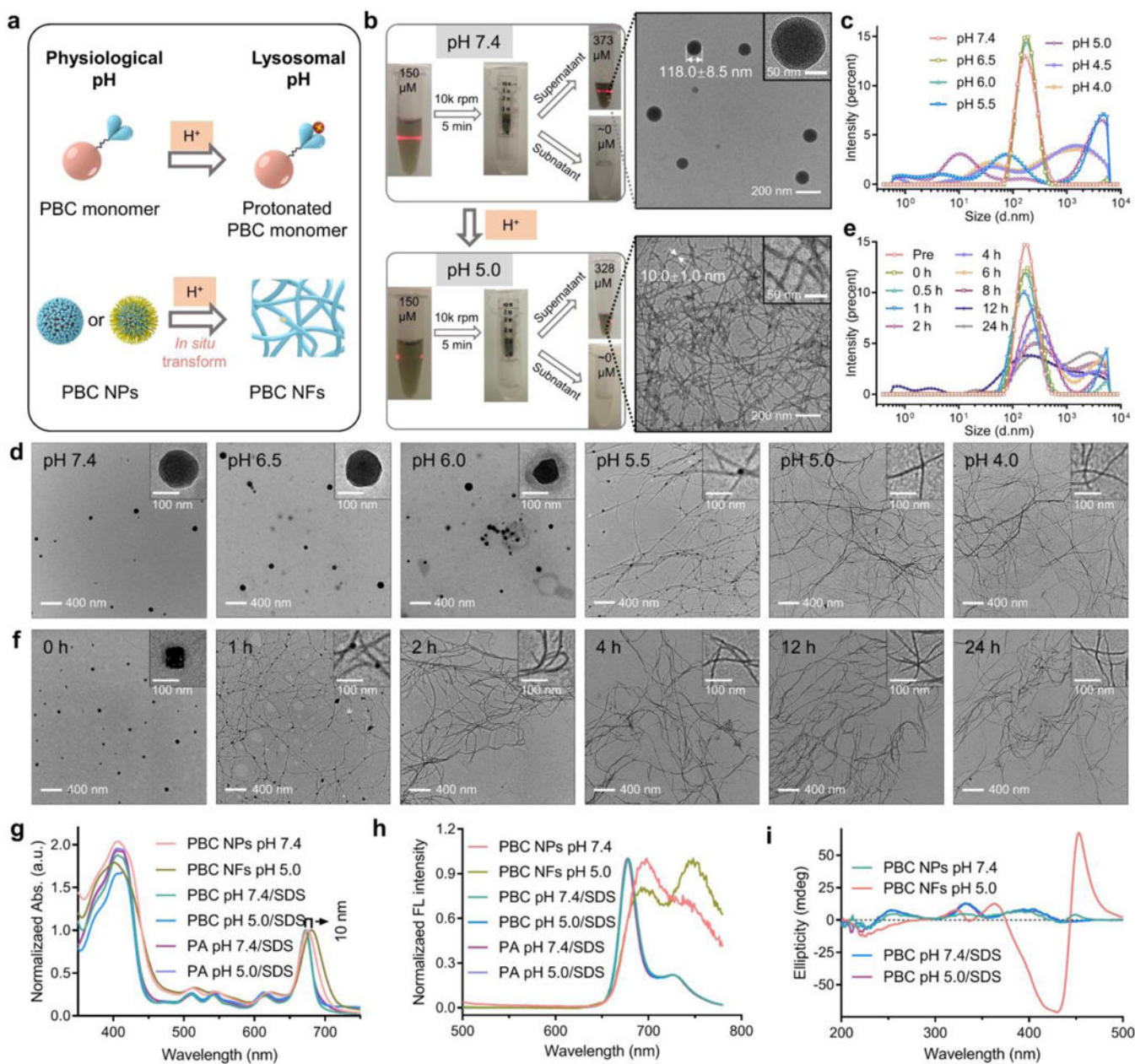
Figure 2.
PBC NPs undergo a pH-responsive phase transformation. a) Schematic illustration of protonation states of PBC under various pH and the resulting forms of aggregates. b) Ultrafiltration analysis and TEM images showing that two different types of PBC aggregates (NPs and NFs) were present at pH 7.4 or pH 5.0, respectively. Scale bar: 200 nm (large picture), 50 nm (inset). c, d) pH-dependent changes of the size distribution (c) and ultrastructural morphology (d) of PBC NPs. Samples were incubated in the PBS solutions of a pH gradient for 24 h before the testing. Scale bar: 400 nm (large picture), 100 nm (inset). e, f) Time-course changes of the size distribution (e) and ultrastructural morphology (f) of PBC NPs. Samples were incubated at pH 5.0 for the predetermined time slots before testing. Scale bar: 400 nm (large picture), 100 nm (inset). g, h) Normalized absorption spectra (g)

and fluorescence spectra (h) of PBC NPs, PBC NFs, free PBC molecules (with SDS), and free PA molecules (with SDS), respectively. i) Circular dichroism spectra of the free PBC molecules (with SDS), PBC NPs, and PBC NFs.
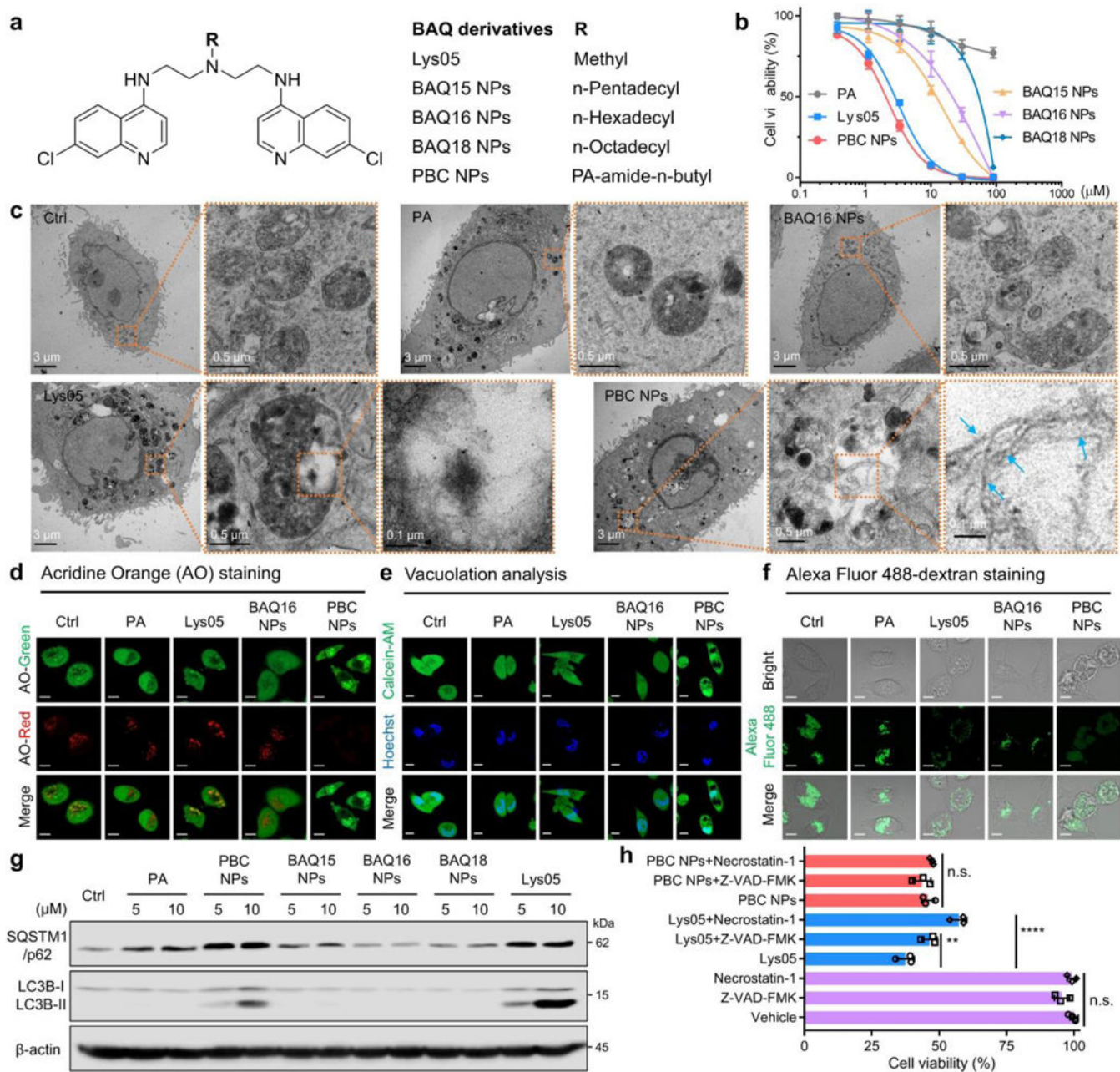
Figure 3.
Transformation of PBC NPs induces lysosomal dysfunction and causes cancer cell death. a)
Chemical structures of BAQ derivatives. b) Cell viability curves. OSC-3 cells were exposed
to the indicated treatments for 48 h. Data are means ± SD (n = 3). c) Representative TEM
images displaying the presence of PBC NFs in the lysosome and the changes of lysosomal
morphology. OSC-3 cells were exposed to the individual treatment (5 μM) for 4 h. Arrow:
PBC NFs. Scale bar for Ctrl, PA, and BAQ16 groups: 3 μm (left), 0.5 μm (right); Scale bar
for Lys05 and PBC groups: 3 μm (left), 0.5 μm (middle), 0.1 μm (right). d) OSC-3 cells were
treated as indicated (5 μM) for 12 h and then were stained with AO. Scale bar: 10 μm. e)
OSC-3 cells were treated as indicated (10 μM) for 16 h and then stained with Calcein AM

and Hoechst 33342. Scale bar: 10 μm. f) Alexa Fluor 488-Dextran-loaded OSC-3 cells were exposed to the individual treatment (10 μM) for 16 h. Scale bar: 10 μm. g) Immunoblotting of OSC-3 cells treated as indicated for 12 h. h) Cell viability of OSC-3 cells that were treated with PBC NPs (2 μM), Lys05 (2 μM), or their combination (Necrostatin-1: 10 μM, Z-VAD-FMK: 40 μM) for 48 h. Data are present as mean ± SD (n = 3).
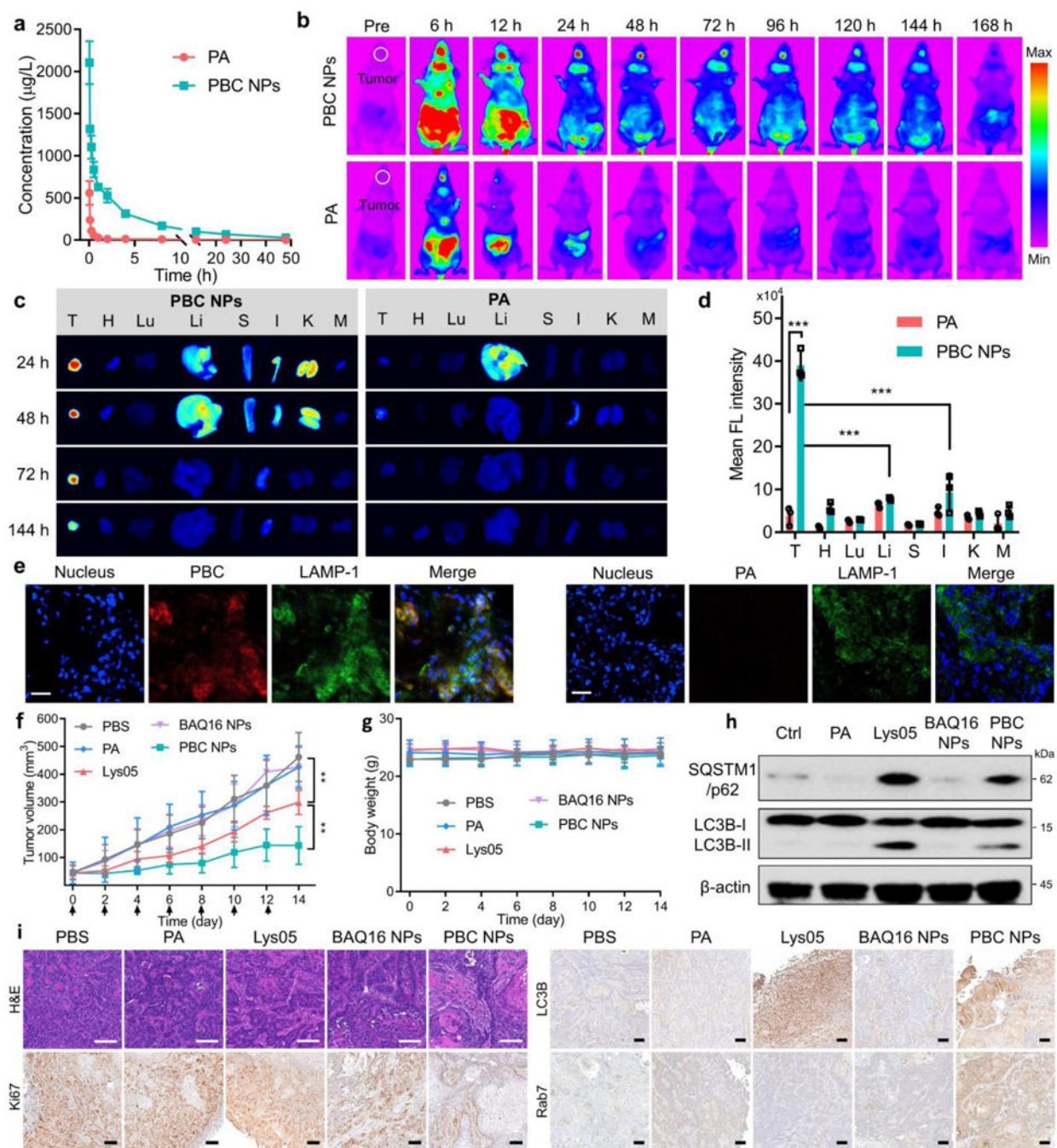
Figure 4.

PBC NPs show prolonged retention in tumors and remarkably suppress tumor growth in vivo. a) Plasma concentration-time profiles of PBC NPs and PA after intravenous injection. Data are presented as means ± s.d., n = 3. b) Time-dependent *in vivo* imaging of mice bearing an orthotopic OSC-3 tumor. c) Time-dependent *ex vivo* imaging of tumors (T), heart (H), lung (Lu), liver (Li), spleen (S), intestine (I), kidney (K), muscle (M), which were collected at 24 h, 48 h, 72 h, and 144 h post-injection. d) Fluorescence quantitative analysis of tumors and main organs that were collected at 72 h post-injection. Data are

presented as means ± s.d., n = 3. Statistical significances were calculated by two-tailed unpaired Student's *t*-test. e) Confocal images of cryosection of harvested OSC-3 tumors at 24 h post-injection of 20 mg/kg PBC NPs or PA. Scale bar: 50 μm. f) Tumor volumes of orthotopic OSC-3 xenografts. Mice were treated as indicated (20 mg kg^{-1}) every 2 days. Data were presented as mean ± s.d., n = 6 tumors from six independent mice. Statistical significances were calculated by two-tailed unpaired Student's *t*-test. g) Average mice bodyweight of different treatment groups. Data were presented as mean ± s.d., n = 6 mice. h, i) Representative immunoblotting analysis (h), histological assays (i) of OSC-3 xenografts from indicated groups. Arrows in g refer to PBC NFs. Scale bar: 100 μm.
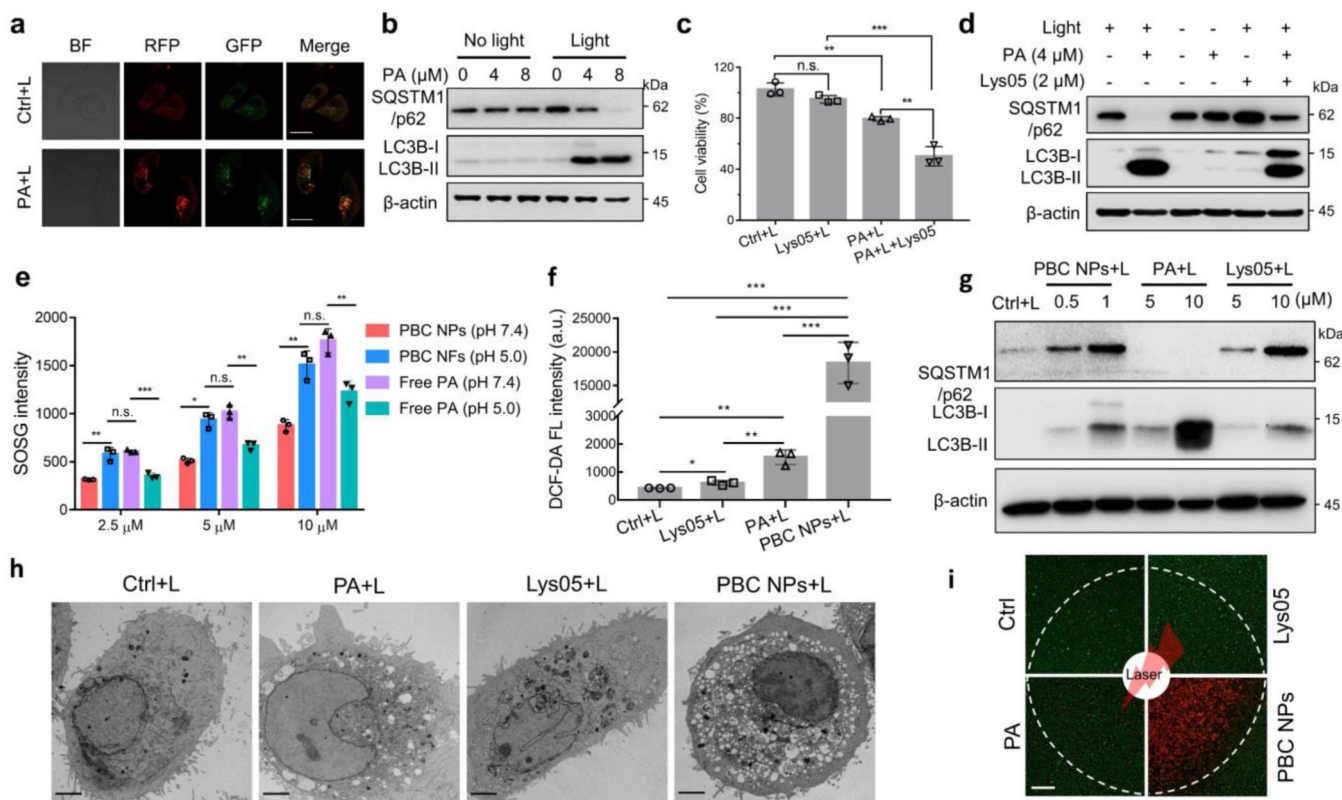
Figure 5.

PBC NPs overcome the inherent autophagy-induced treatment resistance of phototherapy. a, b) Representative imaging (a) and immunoblotting (b) results displaying autophagy induction of the conventional phototherapy. OSC-3 cells expressing GFP-RFP-LC3B (a) or not (b) were incubated as indicated for 24 h, followed by 30 s of light illumination or not and another 24 h culture. Scale bar: 20 μm. c) Cell viability showing synergistic effects between the conventional phototherapy and autophagy inhibition. OSC-3 cells were treated as indicated (Lys05: 1 μM, PA: 2.5 μM) for 24 h, followed by 30 s of light irradiation and another 24 h culture. Data are presented as means ± s.d., n = 3 independent experiments. Statistical significances were calculated by two-tailed unpaired Student's *t*-test. d) Immunoblotting results indicating the synergy mechanism. OSC-3 cells were treated as indicated, followed by 30 s of light irradiation and another 24 h incubation. e) Singlet oxygen production in solution induced by photo-triggered PBC and PA. The solutions containing were incubated with 5 μM SOSG, followed by light irradiation. Data are presented as means ± s.d., n = 3 independent experiments. f) Intracellular ROS production assay. OSC-3 cells were incubated with the individual group (2 μM, 24 h), followed by 30 s of light irradiation and another 4 h culture prior to ROS measurements using DCF-DA as an indicator. Data are presented as means ± s.d., n = 3 independent experiments. Statistical significances were calculated by two-tailed unpaired Student's *t*-test. g) Immunoblotting analysis. OSC-3 cells were incubated as indicated for 24 h, followed by 30 s of light illumination and another 24 h culture. h) Representative TEM micrographs displaying the accumulation of autophagic vesicles. OSC-3 cells were treated as indicated (2 μM, 24 h), followed by 30 s of light irradiation and another 4 h incubation. Scale bar: 3 μm. i) Imaging

analysis of live and dead OSC-3 cells. Cells were treated with the individual agent, followed by 30 s of light irradiation and another 4 h incubation as well as staining with 40 nM of DiOC6(3) (Green) and propidium iodide (Red). Scale bar: 200 μm. "L" in the related panels refers to "light treatment".
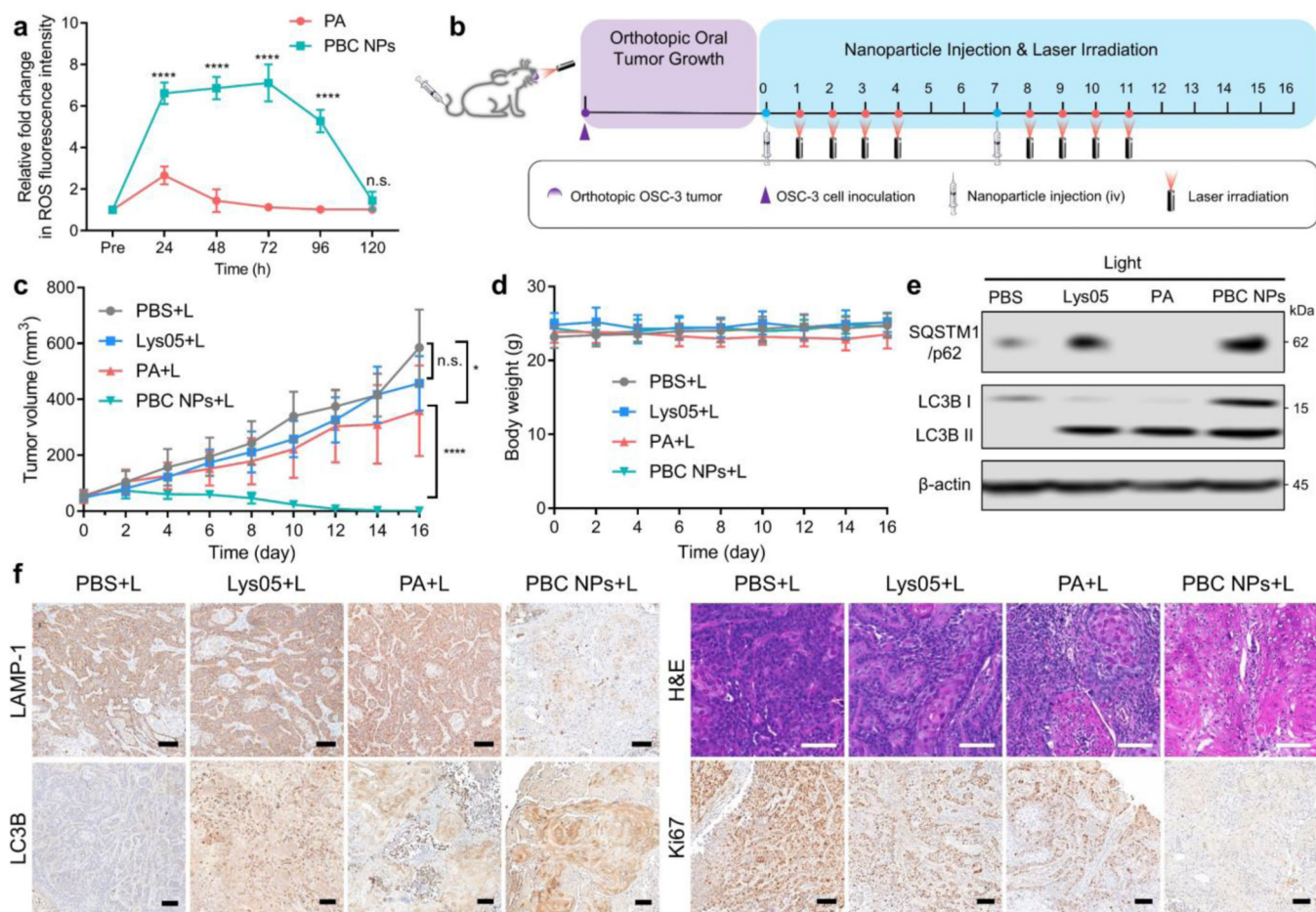
Figure 6.
PBC NPs efficiently facilitate the ablation of orthotopic oral tumors through improved phototherapy. a) ROS levels in orthotopic oral tumors. Mice were injected with single-dose PBC NPs or PA (10 mg kg^{-1}) by tail vein, and tumors were illuminated by laser at the predetermined intervals post-injection, collected and stained with DCF-DA immediately for fluorescence imaging. Data were presented as mean ± s.d., n = 3 tumors from three independent mice per group. b) Schematic illustration of orthotopic OSC-3 tumor inoculation and treatment schedule for mice. c) Tumor volumes of orthotopic oral cancer OSC-3 xenograft. Data were presented as mean ± s.d., n = 6 tumors from six independent mice. Statistical significances were calculated by two-tailed unpaired Student's t-test. d) Average mice bodyweight in different treatment groups. Data were presented as mean ± s.d., n = 6 mice. e, f) Immunoblotting analysis (e) and histological assays (f) of OSC-3 xenografts in the indicated groups. "L" in the related panels refers to "light treatment". Scale bar: 100 μm.